This article was downloaded by: *[Ingenta Content Distribution Psy Press Titles]*
On: *15 May 2011*
Access details: *Access Details: [subscription number 911796918]*
Publisher *Taylor & Francis*
Informa Ltd Registered in England and Wales Registered Number: 1072954 Registered office: Mortimer House, 37-41 Mortimer Street, London W1T 3JH, UK

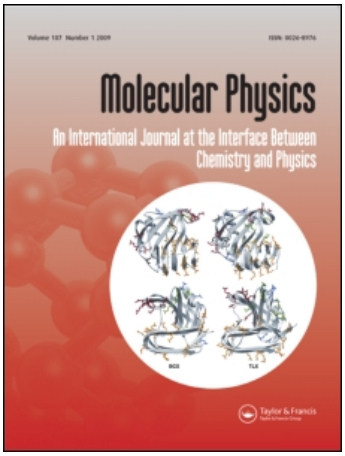

Molecular Physics

Publication details, including instructions for authors and subscription information:
http://www.informaworld.com/smpp/title~content=t713395160

Local structure of liquid-vapour interfaces

Maia Godonoga[a]; Alex Malins[ab]; Jens Eggers[c]; C. Patrick Royall[a]
[a] School of Chemistry, University of Bristol, Bristol, BS8 1TS, UK [b] Bristol Centre for Complexity Science, University of Bristol, Bristol, BS8 1TS, UK [c] School of Mathematics, University of Bristol, University Walk, Bristol, BS8 1TW, UK

Online publication date: 29 April 2011

To cite this Article Godonoga, Maia , Malins, Alex , Eggers, Jens and Royall, C. Patrick(2011) 'Local structure of liquid-vapour interfaces', Molecular Physics, 109: 7, 1393 — 1402
To link to this Article: DOI: 10.1080/00268976.2011.564217
URL: http://dx.doi.org/10.1080/00268976.2011.564217

PLEASE SCROLL DOWN FOR ARTICLE

Full terms and conditions of use: http://www.informaworld.com/terms-and-conditions-of-access.pdf

This article may be used for research, teaching and private study purposes. Any substantial or systematic reproduction, re-distribution, re-selling, loan or sub-licensing, systematic supply or distribution in any form to anyone is expressly forbidden.

The publisher does not give any warranty express or implied or make any representation that the contents will be complete or accurate or up to date. The accuracy of any instructions, formulae and drug doses should be independently verified with primary sources. The publisher shall not be liable for any loss, actions, claims, proceedings, demand or costs or damages whatsoever or howsoever caused arising directly or indirectly in connection with or arising out of the use of this material.

Molecular Physics
Vol. 109, Nos. 7–10, 10 April–20 May 2011, 1393–1402

Taylor & Francis
Taylor & Francis Group

Downloaded By: [Ingenta Content Distribution Psy Press Titles] At: 16:08 15 May 2011

INVITED ARTICLE

Local structure of liquid–vapour interfaces

Maia Godonoga[a], Alex Malins[ab], Jens Eggers[c] and C. Patrick Royall[a]*

[a]*School of Chemistry, University of Bristol, Bristol, BS8 1TS, UK;* [b]*Bristol Centre for Complexity Science, University of Bristol, Bristol, BS8 1TS, UK;* [c]*School of Mathematics, University of Bristol, University Walk, Bristol, BS8 1TW, UK*

(*Received 24 November 2010; final version received 3 February 2011*)

The structure of a simple liquid may be characterized in terms of ground state clusters of small numbers of atoms of that same liquid. Here we use this sensitive structural probe to consider the effect of a liquid–vapour interface upon the liquid structure. At higher temperatures (above around half the critical temperature) we find that the predominant effect of the interface is to reduce the local density, which significantly suppresses the local cluster populations. At lower temperatures, however, pronounced interfacial layering is found. This appears to be connected with significant orientational ordering of clusters based on three- and five-membered rings, with the rings aligning perpendicular and parallel to the interface respectively. At all temperatures, we find that the population of fivefold symmetric structures is suppressed, rather than enhanced, close to the interface.

Keywords: interfaces; liquid structure; simple liquids

1. Introduction

What is the structure of the transition zone between liquid and vapour? In 1893 van der Waals [1,2] described the liquid–vapour interface as a smooth density profile $\rho(z)$, shortly preceded by Rayleigh [3]. Early computational [4] and theoretical work based on the Born–Green–Yvon equation [5] suggested a significant degree of surface layering in the Lennard-Jones model of simple liquids. However, further simulations [6] and density functional theory [2,7] showed that little surface layering is expected for materials based on van der Waals interactions, and that the interfacial profile is dominated by a smooth change in density. Relative to the critical temperature T_c, metals typically remain liquid at rather lower temperatures than Lennard-Jones like materials, and here pronounced surface layering is indeed found [7–11]. An important related problem to the free interface is the confinement introduced by a hard wall, crystal or similar external field, which may be tackled with density functional theory [7,12], simulation [13] and experiment [14,15]. In this case, layering is more generally observed.

In experiments on conventional materials, the measurement of (intrinsic) interfacial profiles is complicated by collective surface excitations in the form of capillary waves [16–19]. For those systems where surface layering is pronounced such as metals, the lengthscale above which capillary wave effects become dominant is around 100 nm. This lengthscale is larger than that typically encountered in computational studies, where capillary waves only cause a small broadening of surface layering [9], but cannot be neglected in experiment. Nonetheless surface layering has been demonstrated in experiments, for example in liquid mercury [20].

A further class of materials which may be directly investigated in real space due to their mesoscopic lengthscale are colloidal suspensions. Most notably, colloid–polymer mixtures exhibit (colloidal) vapour–liquid phase separation [21,22], moreover the hard-sphere interactions that closely approximate such systems are amenable to theory [23]. Here capillary waves have been directly visualized [24]. So far, to our knowledge, interfaces in colloidal systems with long-ranged interactions [25] which can be deeply cooled and might exhibit pronounced layering (the equivalent of metals) have not been studied. However, single-particle resolution enables other approaches to be used. Notably, a method introduced by Chacon and Tarazona [26] which pins a plane to a layer of surface particles indeed revealed density oscillations perpendicular to the pinned surface in a colloidal liquid [27].

Here we consider the perturbation induced by the interface on the liquid structure at the molecular/atomic level. We consider two different liquid systems.

*Corresponding author. Email: paddy.royall@bristol.ac.uk

ISSN 0026–8976 print/ISSN 1362–3028 online
© 2011 Taylor & Francis
DOI: 10.1080/00268976.2011.564217
http://www.informaworld.com

Downloaded By: [Ingenta Content Distribution Psy Press Titles] At: 16:08 15 May 2011

The first is a truncated and shifted Lennard-Jones (LJ) liquid [28,29] whose triple temperature T_{tr}^{LJ} lies at $T_{tr}^{LJ}/T_c^{LJ} = 0.630$ where T_c^{LJ} is the critical temperature. To observe a stronger effect of the liquid–gas interface, we also consider a model potential which approximates sodium (Na), whose triple point lies at a rather lower temperature relative to criticality of $T_{tr}^{Na}/T_c^{Na} = 0.22$ [8,10]. This model is known to exhibit strong surface layering around the triple point, which is also seen in *ab initio* simulations [11].

In the bulk, it is argued that liquid structure is determined to a significant degree by structures which are energetically locally favourable [30]. Such locally favoured structures can correspond to clusters which minimize the potential energy in isolation and may be catalogued and ordered by the number of particles they contain [31–34]. Structures which exhibit fivefold symmetry, in particular, are very common and account for up to 2/3 of all particles [34,35]. As a result, the local dynamics can be determined to a significant degree by the geometry and the symmetries of the locally favoured structures. This observation is potentially significant to understand the glassy behaviour of supercooled liquids: if the symmetry of the locally favoured structure differs from that of the crystalline state, the path to crystallization is frustrated.

It is thus natural to ask what happens to the concentration of clusters near the liquid–gas interface. This will be a significant measure of local liquid structure. Two mechanisms will contribute to a significant change in cluster concentration near the interface. First, structures favoured by the bulk may be suppressed near the free surface. Second, clusters are non-isotropic, and might thus be ordered in a particular way with respect to the free surface. We will explore this ordering effect in the case of two very common clusters, following the nomenclature of Doye *et al.* [31]: the 5A triangular bipyramid and 7A pentagonal bipyramid, which are three- and five-membered rings with atoms attached above and below the plane of the ring.

One might think that the free surface could lead to an *enhancement* of local fivefold symmetry. The reason is that in the case of deeply quenched liquids, the free interface can to an extent be thought of as a constraining field. Now the structure induced in simple liquids by confinement such as hard walls has been shown, under the application of a second field, to induce some fivefold symmetry [36], which may be conjectured to relate to X-ray reflectometry experiments on lead which found evidence for local fivefold symmetry at the interface [37]. Surprisingly, here our analysis suggests the opposite effect: 7A pentagonal bipyramid clusters, which form the basic unit of fivefold symmetry in our methodology [33,34], are suppressed disproportionately near the interface.

To determine locally favoured structures, we use a novel method, the Topological Cluster Classification (TCC). This identifies small clusters of particles from within bulk phases which are topologically similar to a set of reference clusters [33]. In this case the reference structures are formed by groups of $5 \leqslant m \leqslant 13$ Morse particles in isolation [32] and, depending on the range of the Morse potential, correspond to the global energy minimum clusters of the Lennard-Jones and sodium potentials considered. We have recently explored the structure of the bulk Lennard-Jones liquid and a system similar to the sodium model using this method [35]. Contrary to the suggestion of Frank who conjectured that in the structure of such liquids 13-membered icosahedral structures might be prevalent, we found that these only account for one particle in a thousand, according to our criteria. Instead fivefold symmetry stems from pentagonal bipyramids, which account for 54% of the particles at the Lennard-Jones triple point [35].

This paper is organized as follows. First, we describe our methodology for identifying the interface, and local structure in Section 2. We then proceed to present and discuss our findings in Section 3 before placing our findings in context in the concluding Section 4.

2. Methodology

2.1. *Models*

We use the Monte Carlo (MC) method to simulate a liquid in equilibrium with its vapour phase [38]. We use the Lennard-Jones (LJ) 12–6 potential, where, for two particles separated by a distance r, the interaction energy U is given as

$$\beta U_{LJ}(r) = 4\beta\varepsilon_{LJ}\left[\left(\frac{\sigma_{LJ}}{r}\right)^{12} - \left(\frac{\sigma_{LJ}}{r}\right)^{6}\right], \qquad (1)$$

where $\beta = 1/k_B T$ with k_B being Boltzmann's constant and T is temperature. There are two parameters: ε_{LJ} is the strength of the attraction between the particles and σ_{LJ} determines the range of the interaction. From here on we quote all quantities in standard reduced units, where energies and lengths are normalized by ε_{LJ} and σ_{LJ} respectively.

Now the triple point of Lennard-Jones lies around $T_{tr}^{LJ} = 0.68$, so the maximum degree of cooling relative to the critical point is $T_{tr}^{LJ}/T_c^{LJ} = 0.63$. We would like to realize even lower temperatures and this can be achieved by employing models with longer-ranged interactions which freeze at lower temperatures relative

Downloaded By: [Ingenta Content Distribution Psy Press Titles] At: 16:08 15 May 2011

to criticality. In particular, the spherically symmetric model for sodium (Na) introduced by Chacon and co-workers [8,10] has a triple point around $T_{tr}^{Na} = 0.27$ and critical point around $T_c^{Na} = 1.25$, enabling a much larger degree of cooling, $T_{tr}^{Na}/T_c^{Na} = 0.22$. This model potential for sodium reads

$$\beta U_{Na}(r) = \beta A_0 \exp(-ar) - \beta A_1 \exp\left[-b(r - R_1)^2\right], \tag{2}$$

where $A_0 = 437.96\,\text{eV}$, $A_1 = 0.18382\,\text{eV}$, $a = 2.2322$ Å^{-1} $b = 0.2140$ Å^{-2} and $R_1 = 3.5344$ Å. A lengthscale $\sigma_{Na} = 3.48$ Å is defined as the minimum of U_{Na} along with a well depth $\varepsilon_{Na} = U_{Na}(\sigma_{Na}) = 0.1885\,\text{eV}$. Energies and lengths are then normalized by ε_{Na} and σ_{Na} respectively.

In Figure 1 we show the Lennard-Jones and sodium potentials to be considered below. We also display the Morse potential, which will be used as a reference potential for the minimum energy clusters of the sodium model.

We truncate and shift the Lennard-Jones potential at finite range $r_{cut} = 2.5\sigma$ such that $\beta U_{LJ}(2.5\sigma) = 0$. In the case of the model sodium potential, we follow [10] and truncate the model potential at $r_{cut} = 2.5\sigma$ but, unlike the LJ case, we do not shift the potential, i.e. $\beta U_{Na}(2.5\sigma) < 0$.

2.2. *Simulation details*

We use Monte Carlo simulations in the NVT ensemble [38]. The simulations consist of $N = 16,000$ particles in cuboid boxes with sides $L \times L \times 2L$ and with periodic boundary conditions. This geometry ensures that, once equilibrated, the liquid forms a slab with two interfaces perpendicular to the z-direction. Assuming the interface does not overlap with itself, the z-position of the top or bottom interface may be expressed as a function of (x, y).

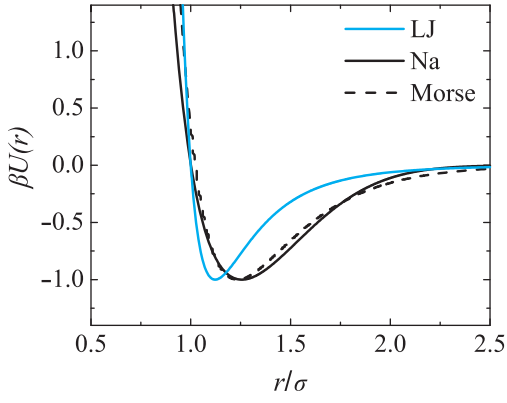

Figure 1. Model potentials used. Blue line, Lennard-Jones (LJ); solid black line, sodium (Na); dashed line, Morse potential with range parameter $\rho_0 = 4.05$.

We present results for two state points in the case of Lennard-Jones $\rho = 0.32$, $T = 0.95$ and $\rho = 0.32$, $T = 0.68$, and in the case of sodium $\rho = 0.485$, $T = 0.542$ and $\rho = 0.485$, $T = 0.270$. These correspond to $T/T_c = 0.880$, 0.630, 0.434 and 0.237 respectively where T_c is the critical point of LJ or Na respectively. ρ is the overall density in the simulation box, which contains both liquid and vapour. This gives $L = 29.2\sigma_{LJ}$ for the LJ state points and $L = 25.5\sigma_{Na}$ for the sodium state points.

For all simulations suitable liquid–vapour coexistence initial configurations are generated by first estimating appropriate bulk liquid ρ_L and vapour ρ_G densities at coexistence from the literature [8,39] and then equilibrating a liquid slab of density ρ_L in coexistence with a vapour at ρ_G for at least 300,000 MC sweeps. Equilibration is ensured by both checking relaxation of the total potential energy and by examining the evolution of the liquid–vapour density profile $\rho(z)$. It has been shown that the coexistence densities and $\rho(z)$ depend on the system size, the geometry of the box, and the boundary conditions of the simulation [40], as well as the truncation length and whether the potential is shifted [39]. Once the density profile $\rho(z)$ is seen to have stopped evolving, we say the system is at equilibrium and a production run of 10,000 MC sweeps is used to generate 100 independent configurations for analysis. Four or more independent simulations are performed for each state point and the results averaged over all eight or more liquid–vapour interfaces obtained from these.

2.3. *Determining the interface location*

To calculate the location of the interface we first fit $\rho(z)$ with a hyperbolic tangent function in the following form

$$\rho(z) = \frac{\rho_L + \rho_G}{2} + \frac{\rho_L - \rho_G}{2} \tanh\left(\frac{z - z_0}{w}\right), \tag{3}$$

where ρ_L and ρ_G are the bulk densities of the liquid and the gas at equilibrium coexistence, w quantifies the width of the interfacial region, and z_0 is the position of the interface with respect to the simulation coordinate axis z. As we will discuss below, w as determined by (3) ignores the effect of capillary waves on the interface. Although it is difficult to accurately decouple the intrinsic width of the interface from that of a capillary broadened interface [40], we show below, for all the state points studied here, ignoring the effects of

Downloaded By: [Ingenta Content Distribution Psy Press Titles] At: 16:08 15 May 2011

capillary broadening and using the fit (3) to determine the position and orientation of the interface, that the conclusions drawn about the structure of the interface do not significantly change as a result of this approximation.

To assess the effect of capillary waves, we note that Equation (3) assumes that the interface position is independent of the local x, y position and is perfectly flat, which is clearly not the case if capillary waves are present. We imagine that the interfacial width may be decomposed into capillary-broadened and intrinsic components w_{cw} and w_{i} where $w = w_{\mathrm{cw}} + w_{\mathrm{i}}$ and we are interested in the intrinsic width w_{i} [41]. We determine the effect of surface roughening (capillary waves) as follows [42]. Firstly we divide the simulation cube into n^2 columns of width and breadth L/n and height L for integer n as shown in Figure 2. Rather than Equation (3), we model the density profile $\rho_{i,j}(z)$ of column i, j with the step function

$$\rho_{\mathrm{step}}(z) = \begin{cases} \rho_{\mathrm{L}}, & z < z_{0,i,j}, \\ \rho_{\mathrm{G}}, & z \geq z_{0,i,j}, \end{cases} \tag{4}$$

where $z_{0,i,j}$ is the position of the interface and i and j are integers denoting the column. We minimize the least-squares residuals between $\rho_{i,j}(z)$ and $\rho_{\mathrm{step}}(z)$ to find $z_{0,i,j}$.

Re-scaling the z axis as $\rho_{i,j}(z - z_0)$ gives columnar density profiles centred on the position of the interface. Taking the mean of these columnar profiles gives $\rho_{\mathrm{av}}(z - z_0)$ the averaged density profile with capillary waves at and above the columnar scale removed, which we then fit with the tanh function (3) leading to a new interfacial width w_n. Due to capillary broadening, the square of the measured interfacial width has a logarithmic dependence on the column width [41], while extrapolating the column width to zero gives an estimate of the intrinsic width. However, for very small column widths, there are insufficient statistics (coordinates) in the columns to reliably give the columnar density profiles $\rho_{i,j}(z - z_0)$.

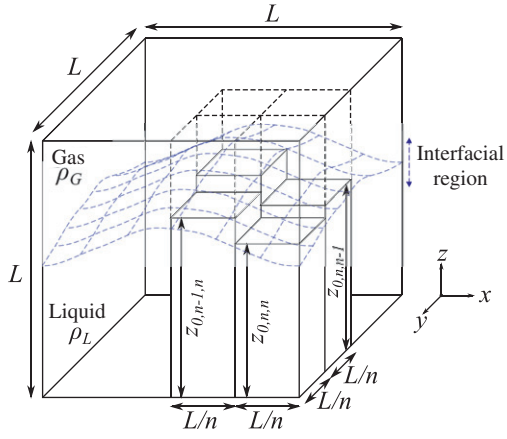

Figure 2. Identification of the position of a capillary perturbed interface. The interface is shown in blue and the cube is split into n^2 columns i, j. The interface is assumed flat in each column and the position is extracted by a fitting step function (Equation (4)) to the columnar density profile $\rho_{i,j}(z)$. Note periodic boundaries apply in the x and y directions only.

For the LJ $T = 0.95$ state point, where we expect the largest contribution w_{cw} from capillary waves, the minimum we obtain is $w_n = 2.11(1)\sigma_{\mathrm{LJ}}$, compared to the flat-interface value of $w = 2.38(2)\sigma_{\mathrm{LJ}}$. w as obtained from Equation (3) is only slightly (around 10%) larger than the minimum w_n obtained from the capillary wave analysis and therefore roughening of the interface is minimal over the lengthscale we measure. Following this analysis we conclude capillary waves make a rather limited impact on the interfacial widths we can measure and hereafter neglect the effect of capillary waves and simply fit the whole simulation box with Equation (3) to determine the location of the interface. We henceforth rescale our z-axis such that $z_0 = 0$.

2.4. *Topological cluster classification (TCC)*

To analyse the structure, we first identify the bond network using a modified Voronoi construction with a maximum bond length $r_{\mathrm{cut}} = 1.8\sigma$ and four-membered ring parameter $f_{\mathrm{c}} = 0.82$ [33]. Having identified the bond network, we use the topological cluster classification to determine the nature of the cluster. This analysis identifies all the shortest path three, four and five membered rings in the bond network. These rings form the basic building blocks of our analysis. A three-membered ring with atoms bound above and below is identified as a 5A triangular bipyramid, a four-membered ring with two bound atoms as a 6A octahedron and a five-membered ring as a 7A pentagonal bipyramid, as shown in Figure 3. The additional atoms bonded to the rings are termed spindle atoms. Now the ground state clusters for Lennard-Jones are known [32], but we are unaware of any work identifying ground state clusters for the sodium model employed here. However, ground state clusters for the variable range Morse potential have been calculated [31]. We therefore *assume* that the clusters of the Morse potential with the relevant range (as discussed below) are also ground states for sodium. We then use the TCC to find clusters which are global energy minima of the Lennard-Jones and Morse potentials, applying the latter to our sodium results. Supporting this

Downloaded By: [Ingenta Content Distribution Psy Press Titles] At: 16:08 15 May 2011

assumption is work which shows that for a model for sodium with many-body interactions, the Gupta model, the ground state clusters are the same as those we infer for the Chacon and Tarazona model [43,44].

The Morse potential is defined

$$\beta U_{\mathrm{M}}(r) = \beta\varepsilon_{\mathrm{M}} \exp[\rho_0(\sigma - r)](\exp[\rho_0(\sigma - r)] - 2), \quad (5)$$

where ρ_0 is a range parameter and ε_{M} is the potential well depth. The Morse potential has a variable range and we choose the range such that it closely approximates the sodium model. The extended law of corresponding states [45] provides a means by which different systems may be compared with one another, by equating their reduced second virial coefficients

$$B_2^* = \frac{B_2}{\frac{2}{3}\pi\sigma_{\mathrm{EFF}}^3}, \quad (6)$$

where σ_{EFF} is the effective hard sphere diameter and the second virial coefficient

$$B_2 = 2\pi \int_0^\infty \mathrm{d}r\, r^2[1 - \exp(-\beta U(r))]. \quad (7)$$

The effective hard sphere diameter is defined as

$$\sigma_{\mathrm{EFF}} = \int_0^\infty \mathrm{d}r[1 - \exp(-\beta U_{\mathrm{REP}}(r))]. \quad (8)$$

Varying the Morse range parameter such that B_2^* for sodium and the Morse potential are equal gives $\rho_0 = 4.05$. Now the ground state minima for the Morse potential are known [31] and here we assume those for $\rho_0 = 4.05$ also hold for $U_{\mathrm{Na}}(r)$. The potentials are compared in Figure 1. We identify all topologically distinct Morse ($\rho_0 = 4.05$) and Lennard-Jones clusters [32]. In addition, we identify the FCC and HCP 13 particle structures in terms of a central particle and its 12 nearest neighbours. We illustrate these clusters in Figure 3. In the case of the Morse potential, for $m > 7$ there is more than one cluster which forms the ground state, depending on the range of the interaction [31]. We therefore consider ground state clusters for each system and for $m < 14$. For more details see [33].

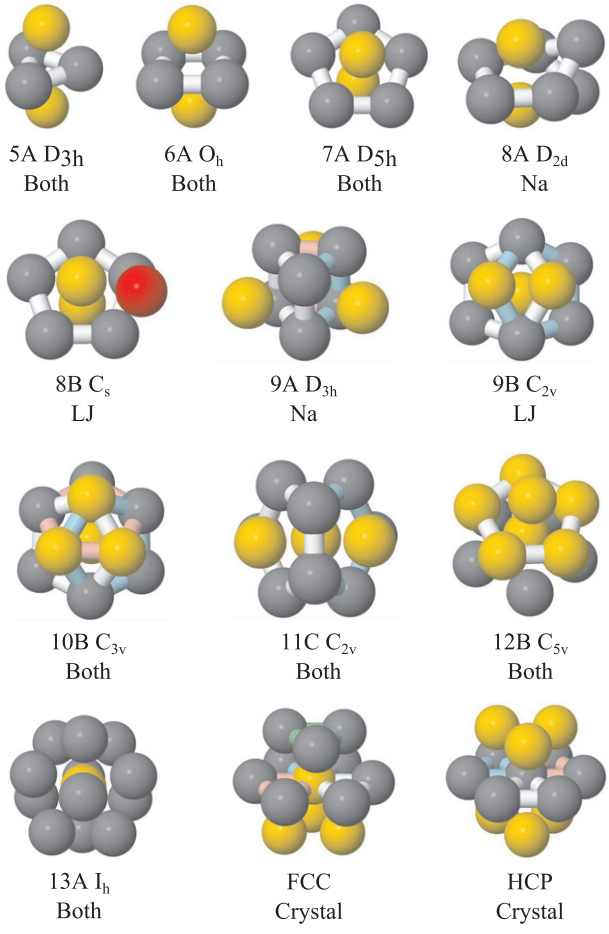

Figure 3. Structures of LJ and Na clusters, nomenclature following [31], and their point group symmetries. The colours denote the method used for cluster detection by the TCC algorithm: three-, four- and five-membered ring atoms are grey, spindle atoms are yellow, additional atoms to a basic cluster are red (here just 8B which is detected from 7A clusters), and rings are coloured white, blue, pink and green.

3. Results

We begin our presentation of the results by showing the interfacial profiles of the different systems and state points. In Figure 4 we see that the interfacial width

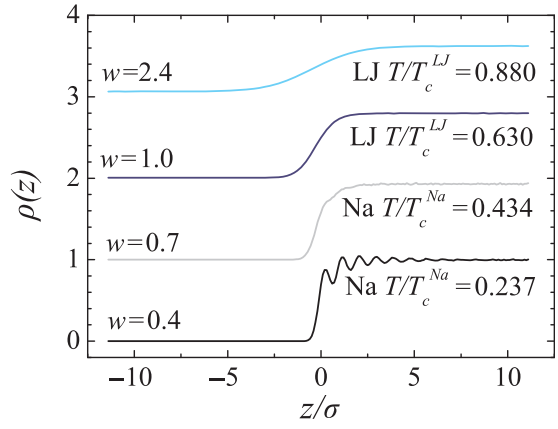

Figure 4. Interfacial profiles $\rho(z)$. From top, Lennard-Jones $T = 0.95$, $T = 0.68$, sodium $T = 0.542$, $T = 0.297$. Data offset for clarity. The sodium interface at the lowest temperature shows a very pronounced surface layering. The interfaces have all been centred at $z = 0$.

Downloaded By: [Ingenta Content Distribution Psy Press Titles] At: 16:08 15 May 2011

drops with decreasing T/T_c. The lowest temperatures, and thus the smallest interfacial widths, are realized for the sodium system. We note the pronounced interfacial layering at the lowest temperature [8,10]. This indicates that the effect of the interface on the local ordering of the liquid extends far into the bulk in that case.

We now proceed to the TCC analysis of the Lennard-Jones liquid at two different temperatures. We plot the total density of particles $\rho(z)$ as well as the particle densities $\rho_C(z)$ for the most popular clusters. These are defined as the densities of all the particles belonging to a particular cluster. The densities are plotted on a logarithmic scale as a function of the distance z from the interface in Figure 5. Note that the liquid side only is plotted ($z > 0$), and that, for Lennard-Jones, the density varies smoothly across the interface for our treatment [8,10]. For each of the temperatures, we also plot the cluster densities *relative* to the total density on a linear scale. The relative density is then defined as the density of particles in a given cluster $\rho_C(z)$ divided by the total density $\rho(z)$. In the bulk it is seen that the most popular clusters, including the 7A pentagonal bipyramid, account for more than half of all the particles.

As one moves towards the interface, the relative density of clusters decreases. For the Lennard-Jones system, our analysis suggests that there is no enhancement of fivefold symmetry at this interface. In fact, as all cluster populations drop with the reducing density at the interface, we argue that there is more of a reduction in fivefold symmetry than anything else. In particular the 7A pentagonal bipyramid cluster may be taken as a rough proxy for five-membered rings, the basic unit of fivefold symmetry. These clearly follow the density profile, although the increase with depth into the liquid is much more marked than the overall density. Similar conclusions can be drawn about the 13A icosahedron. The decrease in relative cluster density can be rationalized by observing that while potential energy considerations enhance cluster populations [35], so too does packing [33]. Thus we expect a decrease in cluster population at lower density, for example upon approach to the interface.

For example, for both $T = 0.95$ ($T/T_c^{LJ} = 0.880$) and $T_{tr}^{LJ} = 0.68$ ($T/T_c^{LJ} = 0.630$), the relative decrease in density amounts to a factor of two in the case of 7A pentagonal bipyramid clusters. Since the change appears coupled to the overall density ρ, we see further change in the structure of the liquid near the surface for the temperatures studied. Note that although it would be attractive to investigate the effect of reducing the density on the cluster population in a bulk system

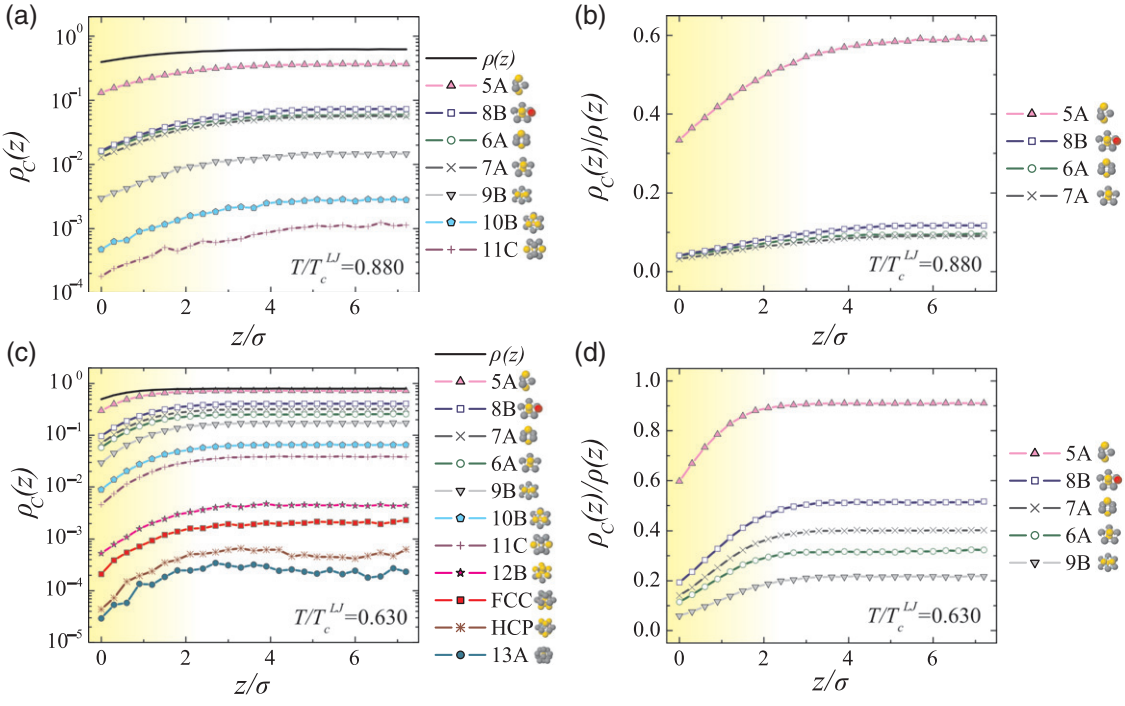

Figure 5. TCC analysis of the Lennard-Jones interface $\rho_C(z)$ denotes the density of particles belonging to a particular cluster type. $\rho(z)$ reproduces the data in Figure 4. (a) $T = 0.95$ ($T/T_c^{LJ} = 0.880$). (c) The triple point $T_{tr}^{LJ} = 0.68$ ($T/T_c^{LJ} = 0.630$). (d) Same data as (c) but normalized by $\rho(z)$. Interface increases from $z = 0$, black interface density profile. Yellow shading is a guide to the eye, indicating the width of interfacial region.

Downloaded By: [Ingenta Content Distribution Psy Press Titles] At: 16:08 15 May 2011

of course this is not possible because the Lennard-Jones system would be unstable to vapour–liquid phase coexistence.

To gain more insight into the effect of the interface on the cluster population, it would therefore be desirable to make the effect of the interface more pronounced by going to lower temperatures, thus making the interface sharper [for which we use the model sodium potential Equation (2)]. Note that the triple point in general has a rather higher population of clusters than does $T = 0.95$, which is not unreasonable, as in addition to the higher density the enhanced relative attractions at reduced temperature would be expected to promote clustering, which has been observed in the bulk [46].

We next performed the same spatially resolved cluster analysis for sodium at lower temperatures relative to criticality. We confirmed that, at higher $T_{\mathrm{tr}}^{\mathrm{Na}} = 0.63$, the results with sodium were very similar to those for Lennard-Jones. As Figure 4 has shown, the interface becomes narrower and at the lowest temperature there are oscillations of the bulk density profile indicating significant surface layering. This shows that the interface changes structuring into the liquid at longer ranges than in the case of Lennard-Jones.

Once more we first show the absolute densities for all the clusters on a logarithmic scale, and then the densities relative to the total on a linear scale (Figure 6). The latter are a direct measure of the influence of the interface on the local ordering. At the higher temperature, the decrease in the relative cluster density is more pronounced than before, but still remains modest. We note that once more there is certainly no *increase* of 7A pentagonal bipyramid cluster concentration owing to orientational ordering near the interface.

At the lower temperature, 7A clusters account for 82% of the particles in the bulk, the relative density is reduced to 31% near the interface, a somewhat larger drop in population. However, in stark contrast to the higher temperature state points, the effect on cluster concentration extends far beyond the density decrease related to the interface, and into the bulk. This mirrors the layering as reflected in the oscillations of the density profile. The cluster concentrations are evidently a sensitive measure of the layering effect, and of the change in orientational order it introduces.

By contrast, the relative decrease of the triangular bipyramidal 5A clusters is relatively mild. As the clusters are smaller, this might be expected, since the perturbation by the interface on the compact 5A structure will be smaller. Other popular clusters, notably 6A octahedra and 8A D_{2d} also show a similar behaviour. To gain more insight into the concentration

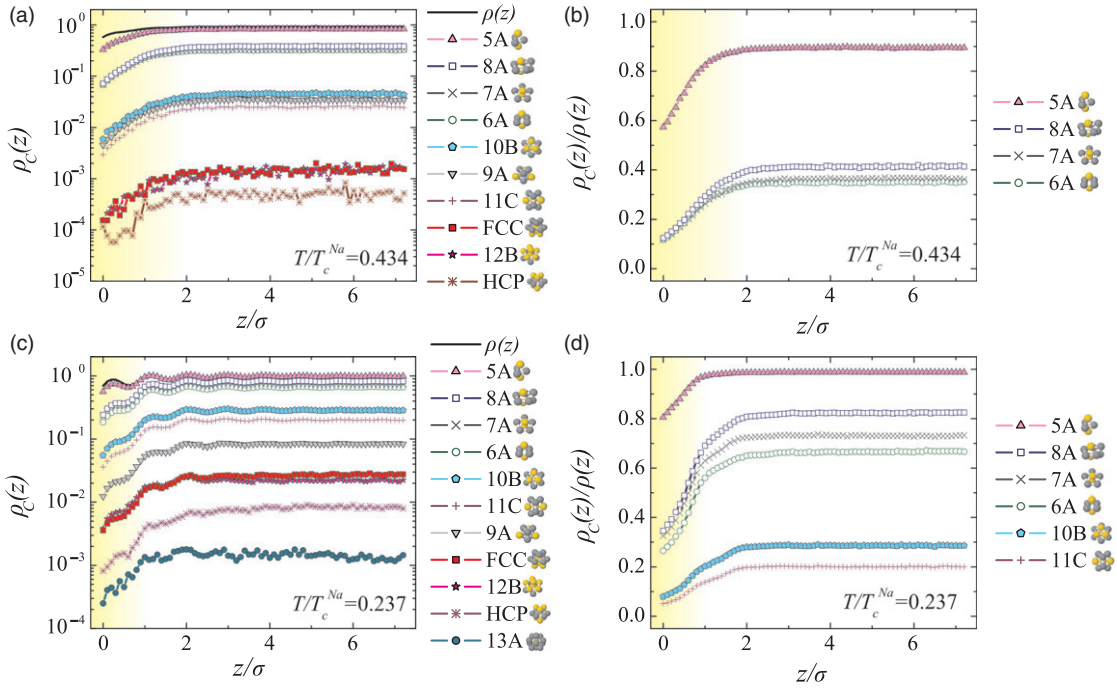

Figure 6. TCC analysis of the sodium interface $\rho_C(z)$ denotes the density of particles belonging to a particular cluster type. $\rho(z)$ reproduces the data in Figure 4. (a) $T = 0.542$ ($T/T_c^{\mathrm{Na}} = 0.434$). (c) Near the triple point $T_{\mathrm{tr}}^{\mathrm{Na}} = 0.297$ ($T/T_c^{\mathrm{Na}} = 0.237$). (b) and (d) Same data as (a) and (c) but normalized by $\rho(z)$. Yellow shading is a guide to the eye and indicates the interfacial region.

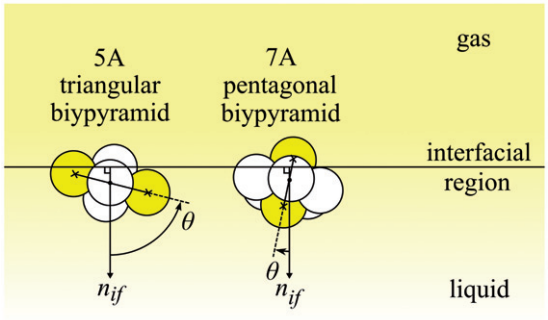

Figure 7. Definition of the orientational order parameter used in the case of the 5A triangular bipyramid and 7A pentagonal bipyramid. θ is the angle between the normal n_{if} to the plane of the interface (marked in blue) and the vector connecting the centres of the yellow spindle atoms.

of 5A and 7A clusters, we consider their orientational ordering near the interface. As seen in Figures 3 and 7, both are viewed as a three-membered and five-membered ring, respectively, with two spindle particles sticking out in a direction perpendicular (ignoring thermal fluctuations) to the ring. We neglect the 6A octahedron due to its high symmetry. To measure the orientation of these structures relative to the interface, we consider the angle θ between the spindle particles and the normal to the plane. From this we can construct an order parameter $1/2\langle 3\cos^2\theta - 1\rangle$ which is zero in the bulk, where all orientations are equal, unity in the case that all clusters are aligned with the axis perpendicular to the interface and $-1/2$ when clusters lie with the axis parallel to the interface.

In Figure 8 we plot the order parameter as function of z for both 5A and 7A clusters for three different T/T_{c} ratios. Remarkably, the two types of clusters behave in an opposite way near the interface. While the 7A clusters are aligned with the five-membered ring parallel to the interface, the 5A clusters are aligned with its three membered ring *perpendicular* to the interface. This effect increases strongly with decreasing temperature, so at that lowest temperature [Figure 8(c)] in the case of 7A the angle θ is reduced, and the order parameter goes to 1/2, half of what would be a perfectly ordered state.

Thus it is likely that the five-membered ring of the 7A clusters tends to be found in the plane of the interface. Assuming that 7A is in a configuration which minimizes bond stretching/compression (i.e. zero-temperature potential energy minimum), this would leave one end of the spindle sticking out from the free surface. This would be an energetically unfavourable situation, which could explain the suppression of 7A clusters near the interface. However the consequences of finite temperature may well play an important role

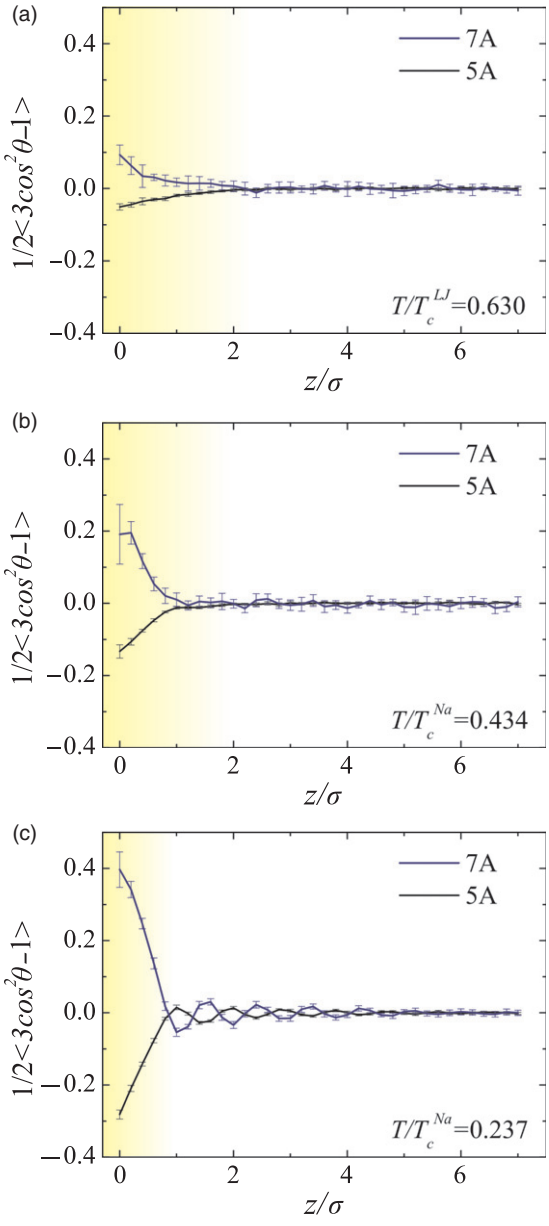

Figure 8. The ordering of the 5A and 7A clusters relative to the interface, as a function of the distance z from the interface. The angle θ is the angle between the vector that connects the spindle particles and the normal to the surface. (a) Lennard-Jones, $T=0.95$, $T/T^{\mathrm{c}}=0.880$; (b) sodium, $T=0.542$, $T/T^{\mathrm{c}}=0.434$; (c) sodium, $T=0.297$, $T/T^{\mathrm{c}}=0.237$.

here, a point to which we return in the next section. The situation is very different for 5A clusters, whose degree of ordering is also rather less pronounced. More crucially, though the ordering is such that the spindle remains in the fluid, while the three-membered ring is oriented parallel to the interface. This permits the cluster to remain inside the fluid relatively undistorted,

Downloaded By: [Ingenta Content Distribution Psy Press Titles] At: 16:08 15 May 2011

and the effect on its concentration remains small. Figure 8(c) also shows that the surface layering is well reflected by the orientational ordering of the clusters.

4. Conclusions

We have shown that our topological cluster classification provides insight into the local liquid structure close to a free interface, and can directly probe for local structures with fivefold symmetry. The analysis we have performed provides no evidence in support of an enhanced fivefold symmetry near the interface, however those fivefold symmetric structures that are present tend to be aligned with five-membered rings parallel to the interface.

At higher temperatures, the predominant effect appears to be related to the lowering in density induced by the interface. This is reflected by a drop in the populations of all the clusters we consider. Upon reducing temperature, the interfacial density profile exhibits layering, and seems to induce a change in cluster population extending well into the dense liquid, long after the mean density is that of the bulk liquid. Thus we argue that our analysis indicates that fivefold symmetry is *suppressed* at the liquid–vapour interface in the systems we have considered.

We use our analysis to reveal orientational information on two basic clusters. Close to the interface, the fivefold symmetric 7A pentagonal bipyramid is oriented with its five-membered ring lying parallel to the interface, conversely the 5A triangular bipyramid is oriented with its three-membered ring perpendicular to the interface. Both these effects are strongly enhanced at lower temperature.

Our analysis is topological in nature. That is to say, the structures identified are based on bonds, and we do not consider structural distortions. In particular, we note that the 7A pentagonal bipyramid, aligned with a surface, might leave a spindle atom exposed. However, for a small amount of strain, this exposed spindle could in fact lie very close to the plane of the five-membered ring. We suspect that it may do so at finite temperature.

We identify two possible extensions of this work. It would be interesting to consider the effect of a wall or similar external field, as an alternative to the free interface. It would also be interesting to investigate the behaviour of clusters other than those which are minimum energy ground states in isolation, for example five-membered rings. We have seen that the population of 7A pentagonal bipyramids is reduced near the interface, the topological basis of our analysis precludes ruling out that an exposed spindle atom might be related to this suppression, although at finite temperature we expect this effect to be small. An extension of our analysis to consider distortions in the clusters identified would be helpful. Both these possibilities will be investigated in the future.

Acknowledgements

Bob Evans is thanked for helpful discussions, Stephen Williams for developing the original implementation of the TCC code, and John Russo for critical reading of the manuscript. Hajime Tanaka is thanked for kindly providing space in his lab for CPR and AM while some of this work was carried out. CPR thanks the Royal Society for funding, AM acknowledges the support of EPSRC grant EP/5011214. This work was carried out using the computational facilities of the Advanced Computing Research Centre, University of Bristol – http://www.bris.ac.uk/acrc/.

References

[1] J.S. Rowlinson, J. Stat. Phys. **20**, 197 (1979).
[2] J.S. Rowlinson and B. Widom, *Molecular Theory of Capillarity* (Clarendon, Oxford, 1982).
[3] Lord Rayleigh, Phil. Mag. **33**, 209 (1892).
[4] C.A. Croxton and R.P. Ferrier, J. Phys. C: Solid State Phys. **4**, 2447 (1971).
[5] C.A. Croxton and R.P. Ferrier, J. Phys. C: Solid State Phys. **4**, 1909 (1971).
[6] M. Rao and D. Levesque, J. Chem. Phys. **65**, 3233 (1976).
[7] R. Evans, in *Fundamentals of Inhomogeneous Fluids*, edited by D. Henderson (Dekker, New York, 1992).
[8] E. Chacon, M. Reinaldo-Falagan, E. Velasco and P. Tarazona, Phys. Rev. Lett. **87**, 166101 (2001).
[9] P. Tarazona, E. Chacon, M. Reinaldo-Falagan and E. Velasco, J. Chem. Phys. **117**, 3941 (2002).
[10] E. Velasco, P. Tarazona, E. Chacon and M. Reinaldo-Falagan, J. Chem. Phys. **117**, 10777 (2002).
[11] B.G. Walker, N. Marzari and C. Molteni, J. Chem. Phys. **127**, 134703 (2007).
[12] H. Lowen, Phys. Rep. **237**, 249 (1994).
[13] M. Heni and H. Lowen, Phys. Rev. E **60**, 7057 (2000).
[14] W.J. Huisman, *et al.*, Nature **390**, 379 (1997).
[15] C-J. Yu, A.G. Richter, A. Datta, M.K. Durbin and P. Dutta, Phys. Rev. Lett. **82**, 2326 (1999).
[16] M. von Smoluchowski, Ann. Phys. **330**, 205 (1908).
[17] F.P. Buff, R.A. Lovett and R.H. Stillinger, Phys. Rev. Lett. **15**, 621 (1965).
[18] R. Evans, Adv. Phys. **28**, 143 (1979).
[19] F.H. Stillinger and J.D. Weeks, J. Phys. Chem. **99**, 2807 (1995).
[20] O.M. Magnussen, B.M. Ocko, M.J. Regan, K. Penanen and P.S. Pershan, Phys. Rev. Lett. **74**, 4444 (1995).
[21] H.N.W Lekerkerker, W.C.K Poon, P.N. Pusey, A. Stroobants and P.B. Warren, Europhys. Lett. **20**, 559 (1992).

Downloaded By: [Ingenta Content Distribution Psy Press Titles] At: 16:08 15 May 2011

[22] W.C.K Poon, J. Phys: Condens. Matter **14**, R859 (2002).
[23] J.M. Brader, R. Evans and M. Schmidt, Mol. Phys. **101**, 3349 (2003).
[24] D. Aarts, M. Schmidt and H.N.W Lekerkerker, Science **304**, 847 (2004).
[25] N. Elsner, C.P. Royall, B.V. Vincent and D.R.E. Snoswell, J. Chem. Phys. **130**, 154901 (2009).
[26] E. Chacon and P. Tarazona, Phys. Rev. Lett. **91**, 166103 (2003).
[27] C.P. Royall, D.G.A.L. Aarts and H. Tanaka, Nat. Physics **9**, 636 (2007).
[28] B. Smit, J. Chem. Phys. **96**, 8639 (1992).
[29] W. Shi and J.K. Johnson, Fluid Phase Equilib. **187–188**, 171 (2001).
[30] F.C. Frank, Proc. R. Soc. London, Ser. A **215**, 43 (1952).
[31] J.P.K. Doye, D.J. Wales and R.S. Berry, J. Chem. Phys. **103**, 4234 (1995).
[32] D.J. Wales and J.P.K. Doye, J. Phys. Chem. **101**, 5111 (1997).
[33] S.R. Williams, preprint Cond.Mat.ArXiV, ArXiv: 0705.0203v1 (2007).
[34] C.P. Royall, S.R. Williams, T. Ohtsuka and H. Tanaka, Nat. Mater. **7**, 556 (2008).
[35] J. Taffs, A. Malins, S.R. Williams and C.P. Royall, J. Phys.: Condens. Matter **22**, 104119 (2010).
[36] M. Heni and H. Lowen, Phys. Rev. E **65**, 021501 (2002).
[37] H. Reichert, *et al.* Nature **408**, 839 (2000).
[38] D. Frenkel and B. Smit, *Understanding Molecular Simulation: from Algorithms to Applications* (Academic, New York, 2001).
[39] A. Trokhymchuk and A. Jose, J. Chem. Phys. **111**, 8510 (1999).
[40] K. Binder and M. Muller, Int. J. Mod. Phys. C **11**, 1093 (2000).
[41] S.W. Sides, G.S. Grest and M-D. Lacasse, Phys. Rev. E **60**, 6708 (1999).
[42] R.L.C. Vink, J. Horbach and K. Binder, J. Chem. Phys. **122**, 134905 (2005).
[43] S.K. Lai, P.J. Hsu, K.L. Wu, W.K. Liu and M. Iwamatsu, J. Chem. Phys. **117**, 10715 (2002).
[44] E.G. Noya, J.P.K Doye, D.J. Wales and A. Aguado, Eur. Phys. J. D **43**, 57 (2007).
[45] M.G. Noro and D. Frenkel, J. Chem. Phys. **113**, 2941 (2000).
[46] J. Taffs, A. Malins, S.R. Williams and C.P. Royall, J. Chem. Phys. **133**, 244901 (2010).

Downloaded By: [Ingenta Content Distribution Psy Press Titles] At: 16:08 15 May 2011